Aerosol and Air Quality Research

TECHNICAL NOTE
https://doi.org/10.4209/aaqr.230008

Characterisation of the Aerodynamic Aerosol Classifier Transfer Function for Particle Sizes up to 5 Micrometres

Special Issue:
2022 Asian Aerosol Conference (AAC 2022) (V)

Simon D. Payne [1*], Tyler J. Johnson [2], Jonathan P.R. Symonds [1]

[1] Cambustion Ltd., Cambridge, UK
[2] Department of Mechanical Engineering, University of Alberta, Edmonton, Alberta T6G 2G8, Canada

ABSTRACT

The Aerodynamic Aerosol Classifier (AAC) classifies particles with the desired aerodynamic diameter by generating opposing centrifugal and drag forces on the particles using rotating concentric cylinders and a clean sheath flow. Particle transmission through the classifier is described by its transfer function, which is an important indicator of classifier performance. Characterisation of the classifier's transfer function improves the accuracy of its common aerosol applications, such as measuring particle size distributions or providing classified particles to other aerosol instruments for calibration or further analysis. This characterisation is commonly achieved experimentally using a tandem set-up of the same classifier. While this approach was previously used to characterise the AAC's transfer function for particle aerodynamic diameters up to 2.4 μm using a nebuliser and a Condensation Particle Counter (CPC), the current study expands the AAC's characterisation up to 5 μm using a condensation aerosol generator and an Optical Particle Counter (OPC). This upper size range is significantly higher than that offered by other common aerosol classifiers, such as the approximate 1 μm upper limit typical of the Differential Mobility Analyser (DMA), and it is well suited to many applications, including OPC calibration, bio-aerosols, drug delivery and inhalation studies, and atmospheric dust analysis. This study found that the AAC maintains its high transmission efficiency (≥ 60%) for particles up to 5 μm and that its transfer function width factor increases (i.e., the distribution becomes narrower) as the aerodynamic diameter increases. Setpoint agreement between two different production AACs remained within 2% over the size range tested. Therefore, the AAC has excellent performance for classifying particles up to 5 μm.

Keywords: Aerodynamic diameter, Aerosol classifier, Micrometre particles, Transfer function

Received: January 11, 2023
Revised: March 15, 2023
Accepted: March 31, 2023

* **Corresponding Author:**
spayne@cambustion.com

Publisher:
Taiwan Association for Aerosol Research
ISSN: 1680-8584 print
ISSN: 2071-1409 online

1 INTRODUCTION

Particle classifiers are used to generate a monodisperse aerosol by selecting a narrow range of particle sizes from a wider underlying distribution. These instruments are often used to determine number-based particle size distributions, characterise particle properties and determine size-resolved collection of particles in filters or other devices.

Electrical mobility instruments such as the Differential Mobility Analyser (DMA) have been used for many years by aerosol scientists to classify particle size. The DMA classifies particles based on their electrical mobility diameter by applying an electric field to induce a known electrostatic force, so that charged particles move across a sheath flow (Knutson and Whitby, 1975). As well as relying on charge conditioning of the input aerosol, the charge state is a distribution that can vary with particle morphology, size and composition (Maricq, 2008; Ku *et al.*, 2011; Xiao *et al.*, 2012; Johnson *et al.*, 2021). As a result of the uncertain single-charge fractions, electrostatic aerosol instruments—which also include the Electrical Low Pressure Impactor, the Aerosol Particle Mass Analyser and the Centrifugal Particle Mass Analyser—are susceptible to measurement errors,

TECHNICAL NOTE
https://doi.org/10.4209/aaqr.230008

as well as additional challenges in most applications from the need to identify and correct for the effects of multiply charged particles.

The Aerodynamic Aerosol Classifier (AAC) developed by Tavakoli and Olfert (2013) uses a centrifugal force and sheath flow between two concentric rotating cylinders to classify particles by their relaxation time, τ, defined as

$$\tau \equiv B_m = \frac{C_c(d_a)\rho_0 d_a^2}{18\mu} \quad (1)$$

where B is the particle mobility, m is the particle mass, ρ_0 is a density of 1000 kg m^{-3}, μ is the viscosity of the gas, d_a is the aerodynamic equivalent diameter of the particle and C_c is the Cunningham slip correction factor. The aerodynamic equivalent diameter is defined as the diameter of a spherical particle with a density of 1000 kg m^{-3} that has the same terminal settling velocity as the particle of interest. The AAC can be thought of as translating the DMA into a rotating frame; there is axial sheath flow, but the radial force is centrifugal rather than electrical, which means there is no dependence on the particle charge state. The AAC selects particles of a single aerodynamic diameter (actually, a narrow range of aerodynamic diameters distributed about its setpoint); for a selected value of d_a, smaller particles remain entrained in the sheath flow while larger particles impact on the inner wall of the outer cylinder. The output is a truly monodisperse aerosol with a high transmission efficiency that in theory is limited only by diffusion and impaction losses (Tavakoli and Olfert 2013).

When pairing the AAC with an external particle detector such as a Condensation Particle Counter (CPC) or electrometer, the aerodynamic size distribution of the particles can be measured (Johnson *et al.*, 2018). The accuracy of this and other AAC applications are based on prior knowledge of the classifier's transfer function, which quantifies the probability of each particle being transmitted through the AAC as a function of aerodynamic diameter. The transmission efficiency, λ_Ω, and transfer function width factor, μ_Ω, are used to characterise non-ideal particle behaviour within the classifier: λ_Ω scales the AAC transfer function integrated area to quantify particle losses such as diffusion and impaction, and μ_Ω scales the transfer function full width at half maximum to quantify its broadening due to particle diffusion and other sources, such as classifier flow effects and setpoint variations. Johnson *et al.* (2018) previously characterised the AAC transfer function for aerodynamic diameter setpoints between 50 nm and 2.4 μm using a tandem AAC (TAAC) setup with nebulised oil sources and a CPC. The current study follows Johnson *et al.*'s (2018) recommendation and uses a TAAC setup with a larger underlying size distribution and an Optical Particle Counter (OPC) to quantify the transmission efficiency and transfer function broadening for particles with aerodynamic diameters up to 5 μm.

Recent applications of the AAC for micrometre-range particles include calibration of OPCs (Horender *et al.*, 2019; Sang-Nourpour and Olfert, 2019; Tran *et al.*, 2020; Vasilatou *et al.*, 2021) and bioaerosol detectors (Lieberherr *et al.*, 2021), as well as filtration efficiency measurements of woven face covering materials commonly worn in public spaces during the COVID-19 pandemic (Payne and Symonds, 2022). Other research areas where accurate classification of micrometre-range particles is valuable include aerosol drug delivery and inhalation studies (Labiris and Dolovich, 2003; Heyder, 2004; Danaei *et al.*, 2018), and atmospheric dust studies (Mahowald *et al.*, 2014; Adebiyi *et al.*, 2023).

2 METHODS

2.1 AAC Transfer Function Characterisation

The AAC transfer function was characterised using the tandem AAC (TAAC) setup shown in Fig. 1. The upstream AAC (AAC 1) was set at a constant aerodynamic diameter ($d_{a,1}^*$), while the downstream AAC (AAC 2) was stepped through the aerodynamic diameter domain of the classified particles ($d_{a,2}^*$), and the number concentration of the twice-classified particles (N_2) was measured by using a Palas Welas 1000H light scattering spectrometer as an OPC. Before and after stepping, AAC 2

TECHNICAL NOTE
https://doi.org/10.4209/aaqr.230008

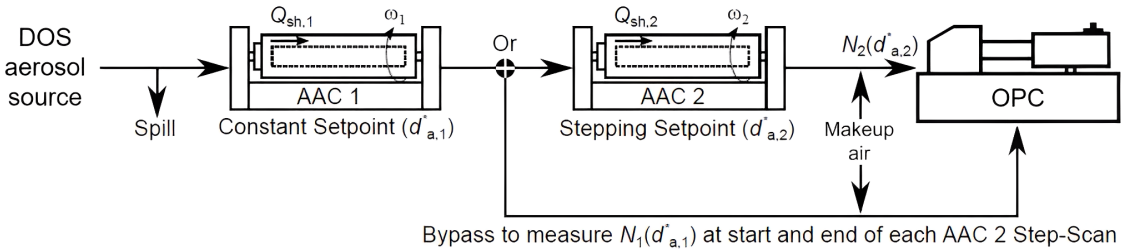

Fig. 1. Tandem AAC experimental setup used to characterise AAC transfer function.

was bypassed to directly measure the particle number concentration passing through AAC 1 (N_1). The aerosol transport tube between AAC 1 and the OPC was the same length as the total tube lengths between AAC 1 and AAC 2 and between AAC 2 and the OPC, so that particle losses in the tubes were consistent and cancel out within N_2/N_1. Therefore, only the particle losses between the AAC inlet and outlet were measured. To compare results from different AACs, the experiments were repeated with the AACs exchanged in position.

At reference classifier conditions (293.15 K and 101,325 Pa), the AAC can classify aerodynamic particle diameters from 32 nm to 3 μm at "low flow" (0.3 L min^{-1} sample flow and 3 L min^{-1} sheath flow) and from 202 nm to 6.8 μm at "high flow" (1.5 L min^{-1} sample flow and 15 L min^{-1} sheath flow) by changing the classifier speed (20–700 rad/s at low flow and 20–500 rad/s at high flow) (Johnson *et al.*, 2018). In the high flow configuration, four different micrometre-range aerodynamic sizes, separated equally in logarithmic space, were selected to characterise the transfer function towards the upper end of the AAC size range. Johnson *et al.* (2018) used a TSI 3775 CPC with an upper particle size limit of 3 μm to measure the number concentration for AAC setpoints up to a maximum of 2.4 μm (so that the AAC 2 could step scan up to 3 μm and characterise the upper side of the distribution classified by AAC 1); in the current study, 2.4 μm was selected as the size range minimum in order to repeat their measurements before continuing to larger aerodynamic diameter setpoints. Since 2018, improved flow forming components at the classifier inlet have been installed in Cambustion's commercial AACs. Previously, jetting of the sample flow at the inlet to the classifier could occur in the high flow configuration, potentially causing transmission of particles outside of the selected aerodynamic diameter at low rotational speeds. The modifications narrowed the flow path that moves radially outwards from the central axis of the two rotating cylinders, so that inlet effects do not persist to the classification region at the annulus. The first repeat measurements at 2.4 μm were obtained using the same nebulised oil source and 3775 CPC to quantify any effect these modifications may have had on the AAC transfer function. TAAC scans at this 2.4 μm AAC 1 setpoint were then repeated using an OPC (rather than a CPC) as the particle counter downstream of the tandem AACs. This repeat verified that the OPC was successful for this application and it was subsequently used for the remaining AAC 1 setpoints of 3.1 μm, 3.9 μm and 5.0 μm. The sample flow of the Palas Welas 1000H is 5 L min^{-1}, which meant 3.5 L min^{-1} make-up air was necessary; this was supplied by a compressed zero air cylinder via a HEPA filter and mass flow controller. At each of the four aerodynamic diameter setpoints, at least five independent AAC 2 step scans were completed, including measuring N_1 prior to (pre-) and after (post-) each AAC 2 scan. To limit uncertainties from instabilities in the generated aerosol, a scan was repeated if the agreement between its pre- or post-N_1 averages was not within 10% and/or the peak-to-peak variation of these measurements was not within 20%.

The transmission efficiency λ_Ω and transfer function width factor μ_Ω were applied within the theoretical triangular AAC transfer function to capture non-ideal behaviour, such as particle diffusion and losses, which follows the approach by Johnson *et al.* (2018) for smaller particles sizes (50 nm to 2.4 μm) and is similar to Martinsson *et al.*'s (2001) characterisation of the DMA transfer function and Naseri *et al.*'s (2023) characterisation of the Centrifugal Particle Mass Analyser transfer function. These factors were determined by fitting the theoretical TAAC convolution through least-squares minimisation to the experimental TAAC data at each setpoint. The minimisation was set to constrain the factors to physical values (i.e., $0 \leq \lambda_\Omega \leq 1$ and $\mu_\Omega \geq 0$), although none of the final results approached these constraints.

TECHNICAL NOTE
https://doi.org/10.4209/aaqr.230008

2.2 Aerosol Source

DOS (bis(2-ethylhexyl) sebacate) was selected as the challenge aerosol, because it forms particles of known spherical morphology and density (914 kg m^{-3}) and has low vapour pressure (i.e., the particles are resistant to shrinkage by evaporation at ambient temperature). A BGI Collison nebuliser previously used by Johnson *et al.* (2018) was the particle generator for repeat measurements at 2.4 μm; subsequently, a Topas SLG 250 was used for all four aerodynamic diameter setpoints (i.e., 2.4 μm, 3.1 μm, 3.9 μm and 5.0 μm). The SLG operates by controlled heterogeneous condensation of DOS vapour onto sodium chloride nuclei according to the Sinclair–La Mer principle. A custom nuclei reduction section with a HEPA filter bypass was added to ensure growth of DOS particles up to 5 μm in aerodynamic diameter for this study and a 5 L mixing chamber was added downstream of the SLG to both dampen temporal instabilities in the aerosol generation process and remove excess liquid.

The SLG generates an aerosol with a narrow size distribution (the geometric standard deviation is generally < 1.2), which presents a challenge for this study since the TAAC convolution fitted to the step scans assumes that the amplitude of the aerosol distribution is constant across the width of the AAC 1 transfer function. The average errors due to this underlying assumption were estimated to be –5.4% for λ_Ω, –2.3% for μ_Ω and +2.4% for τ^*_{12}, the classification agreement between AAC 1 and AAC 2 (i.e., τ^*_1/τ^*_2). Therefore, the transmission efficiency and resolution of the AAC were likely underestimated by the TAAC convolution, though the estimated differences are minor. These estimates were based on applying the theoretical TAAC convolution to the size distribution of the unclassified aerosol measured with the Palas Welas spectrometer, using 1.45 as the refractive index of DOS (Lide, 2001); the estimates are sensitive to the sizing accuracy of the Welas measurements. The Welas was also employed as the OPC for all TAAC scans of aerosol generated by the SLG. A Cambustion rotating disk diluter was used upstream of the TAAC when necessary, so that the particle number concentration remained below the 1×10^4 cm^{-3} coincidence correction threshold of the Welas throughout all experiments (i.e., when measuring N_1 or N_2 in the TAAC setup).

3 RESULTS AND DISCUSSION

3.1 TAAC Scans at 2.4 μm Using Nebuliser and CPC

A comparison of measurements made at d_a = 2.4 μm using the BGI Collison nebuliser as the DOS particle generator and the TSI 3775 CPC as the particle detector is presented in Table 1. All errors quoted henceforth represent the 95% confidence interval (CI) of each average assuming a *t*-distribution. While the transmission efficiency results of Johnson *et al.* (2018) and this study are in good agreement (within 2.5% on average), a narrower distribution (i.e., a 9.2% higher value for μ_Ω on average) than that measured by Johnson *et al.* (2018) was evident in the repeat measurements. Further TAAC scans were run consecutively to check for any significant differences in the transfer function width factor from different combinations of aerosol sources and detectors with the same AAC 1 and AAC 2 units (C and D). The following averages for μ_Ω were obtained: 0.650 ± 0.019 for the Collison nebuliser and 3775 CPC, 0.660 ± 0.032 for the SLG and 3775 CPC and 0.668 ± 0.045 for the SLG and Welas OPC. Since these values are in agreement (within 0.9% on absolute average, indicating good repeatability at 2.4 μm when switching between the nebuliser/SLG and CPC/OPC), it is likely that improved flow forming components at the classifier inlet installed in production AACs since the study by Johnson *et al.* (2018) slightly improved the width of the AAC transfer function. However, the transfer function is still broader than the diffusing log-normal

Table 1. Comparison of transmission efficiency (λ_Ω) and transfer function width factor (μ_Ω) results using the BGI Collison nebuliser and TSI 3775 CPC.

d_a = 2.4 μm, high flow configuration	λ_Ω	μ_Ω
AAC A to B (Johnson *et al.*, 2018)	0.775 ± 0.024	0.617 ± 0.015
AAC B to A (Johnson *et al.*, 2018)	0.803 ± 0.016	0.571 ± 0.006
AAC C to D (this study)	0.823 ± 0.010	0.650 ± 0.019
AAC D to C (this study)	0.795 ± 0.023	0.659 ± 0.019

https://doi.org/10.4209/aaqr.230008

approximation that they calculated and they suggested a classifier flow effect as a possible cause, since greater broadening was observed at higher flows. This effect may involve slight variations in sheath and sample flow distributions around the circumferential position of the classifier, but further work is required to determine if this hypothesis is true. In practice, the user could increase the sheath-to-sample flow ratio as a compensatory measure.

3.2 TAAC Scans at 2.4 µm, 3.1 µm, 3.9 µm and 5.0 µm Using SLG and OPC

Examples of a single TAAC scan for all four aerodynamic diameter setpoints are shown in Fig. 2. The ideal fit represents the scenario if both λ_Ω and μ_Ω were equal to 1, i.e., no particle losses occur in the classifier and there is perfect agreement between the observed broadening of the transfer function and non-diffusing particle streamline theory (Johnson *et al.*, 2018). To account for slight differences in the temperature and pressure of the aerosol between AAC 1 and AAC 2, the equivalent relaxation times and aerodynamic diameters of the AAC-classified particles were calculated at consistent reference conditions (293.15 K and 101,325 Pa) within the TAAC convolution.

The transmission efficiency (calculated as an average of at least five AAC 2 scans at each AAC 1 setpoint) for two different AACs is plotted in Fig. 3 along with the results of Johnson *et al.* (2018).

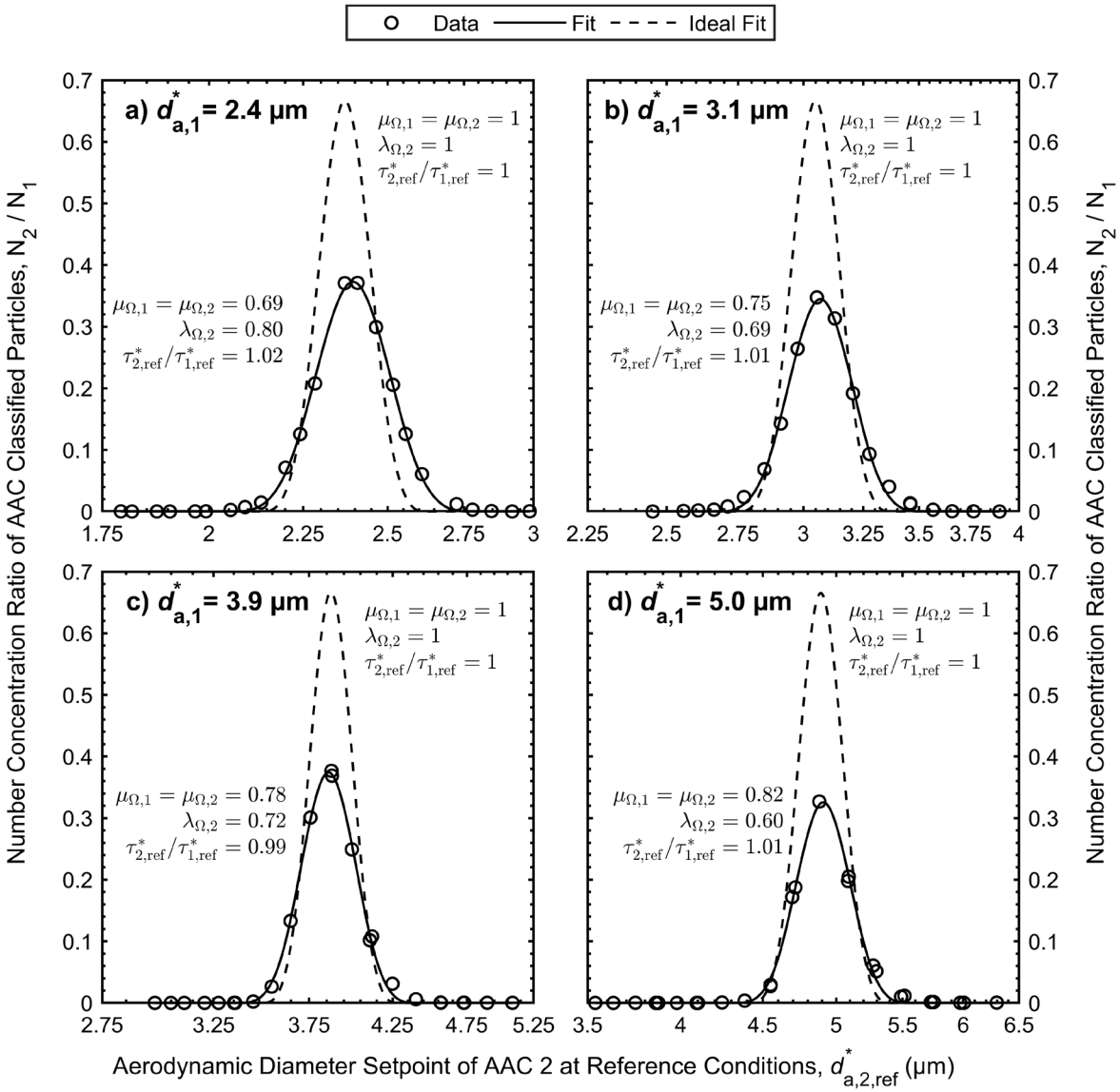

Fig. 2. Representative single tandem AAC scan for each of the four aerodynamic diameter setpoints: a) 2.4 µm, b) 3.1 µm, c) 3.9 µm and d) 5.0 µm.

TECHNICAL NOTE
https://doi.org/10.4209/aaqr.230008

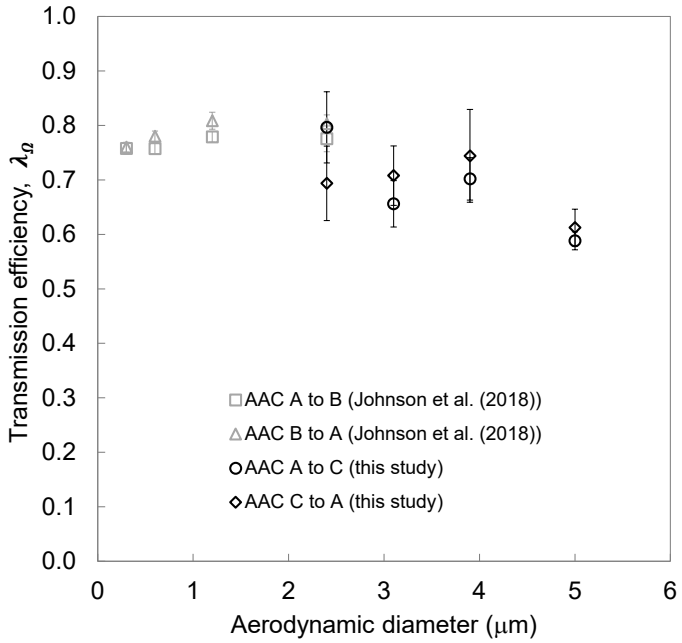

Fig. 3. Transmission efficiency for high flow configuration.

It remains above 60% up to 5 μm for both AACs (units A and C); the transfer functions of units A and B were previously characterised by Johnson *et al.* (2018), prior to modifications to the classifier inlet. The 95% CIs of each average are larger than in the previous experiments by Johnson *et al.* (2018), primarily due to the narrow DOS particle size distribution generated by the SLG. This necessitated longer sampling times during the AAC 2 step scans than with the Collison nebuliser, as well as further repeat experiments to acquire at least five TAAC scans that satisfied the pass criteria (i.e., for which agreement between the pre- and post-N_1 averages was within 10% and the peak-to-peak variation of pre- and post-N_1 was within 20%).

The transfer function width factor plotted in Fig. 4 increases (i.e., the distribution becomes narrower) as the aerodynamic diameter setpoint increases. Therefore, the broadening diminishes as the particle size increases and as the classifier rotational speed decreases. Further investigation is required to explore possible causes, but at faster classifier speeds (and smaller aerodynamic diameter setpoints) it is possible that parallel streamlines in the flow through the classifier may not be as well maintained (especially at the sample inlet and outlet).

Fig. 5 shows the results for the setpoint agreement τ^*_{12} between the 2 production units used in this study. All 8 characterisation points from 2.4 μm to 5.0 μm agree within 2%. This is similar to the 3% or better agreement reported by Johnson *et al.* (2018) for 16 of the 18 characterisation points at aerodynamic diameter setpoints up to 2.4 μm (for both low flow and high flow configurations).

4 CONCLUSIONS

The AAC transfer function was characterised for micrometre-range particle sizes using a tandem AAC set-up with an OPC. These results demonstrate the high transmission efficiency ($\geq$ 60%) of the AAC up to 5 μm and expand its accurate classification range for micrometre size distributions. The width factor of the transfer function increases (i.e., the distribution becomes narrower) as the aerodynamic diameter increases. Setpoint agreement between two different production AACs remained within 2% over the size range tested.

Considerations for future work include characterising the AAC transfer function using non-spherical particles and at different classifier resolutions (i.e., sheath-to-sample-flow ratios), re-characterising the AAC transfer function at smaller particle sizes to account for the changes in inlet geometry, and investigating the causes of the classifier broadening that occur beyond the diffusing particle streamline theory.

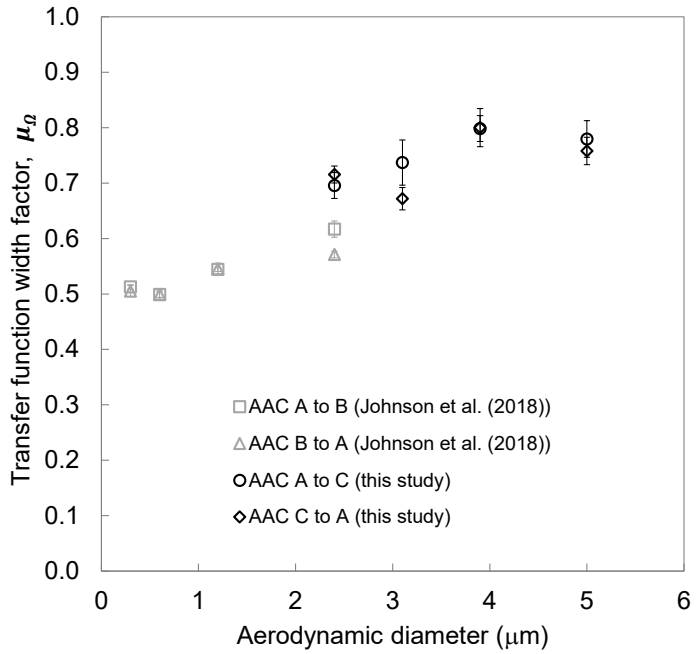

Fig. 4. Transfer function width factor for high flow configuration.

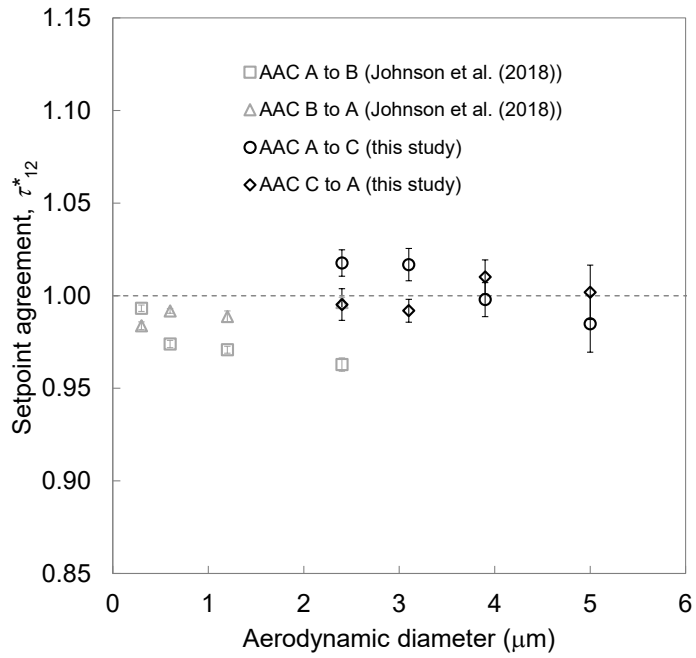

Fig. 5. Classification agreement factor.

REFERENCES

Adebiyi, A., Kok, J.F., Murray, B.J., Ryder, C.L., Stuut, J.B.W., Kahn, R.A., Knippertz, P., Formenti, P., Mahowald, N.M., Pérez García-Pando, C., Klose, M., Ansmann, A., Samset, B.H., Ito, A., Balkanski, Y., Di Biagio, C., Romanias, M.N., Huang, Y., Meng, J. (2023). A review of coarse mineral dust in the Earth system. Aeolian Res. 60, 100849. https://doi.org/10.1016/j.aeolia.2022.100849

Danaei, M., Dehghankhold, M., Ataei, S., Hasanzadeh Davarani, F., Javanmard, R., Dokhani, A., Khorasani, S., Mozafari, M.R. (2018). Impact of particle size and polydispersity index on the

clinical applications of lipidic nanocarrier systems. Pharmaceutics 10, 57. https://doi.org/10.3390/pharmaceutics10020057

Heyder, J. (2004). Deposition of inhaled particles in the human respiratory tract and consequences for regional targeting in respiratory drug delivery. Proc. Am. Thorac. Soc. 1, 315–320. https://doi.org/10.1513/pats.200409-046TA

Horender, S., Auderset, K., Vasilatou, K. (2019). Facility for calibration of optical and condensation particle counters based on a turbulent aerosol mixing tube and a reference optical particle counter. Rev. Sci. Instrum. 90, 075111. https://doi.org/10.1063/1.5095853

Johnson, T.J., Irwin, M., Symonds, J.P., Olfert, J.S., Boies, A.M. (2018). Measuring aerosol size distributions with the aerodynamic aerosol classifier. Aerosol Sci. Technol. 52, 655–665. https://doi.org/10.1080/02786826.2018.1440063

Johnson, T.J., Nishida, R.T., Zhang, X., Symonds, J.P., Olfert, J.S., Boies, A.M. (2021). Generating an aerosol of homogeneous, non-spherical particles and measuring their bipolar charge distribution. J. Aerosol Sci. 153, 105705. https://doi.org/10.1016/j.jaerosci.2020.105705

Knutson, E.O., Whitby, K.T. (1975). Aerosol classification by electric mobility: apparatus, theory, and applications. J. Aerosol Sci. 6, 443–451. https://doi.org/10.1016/0021-8502(75)90060-9

Ku, B.K., Deye, G.J., Kulkarni, P., Baron, P.A. (2011). Bipolar diffusion charging of high-aspect ratio aerosols. J. Electrostat. 69, 641–647. https://doi.org/10.1016/j.elstat.2011.08.006

Labiris, N.R., Dolovich, M.B. (2003). Pulmonary drug delivery. Part I: Physiological factors affecting therapeutic effectiveness of aerosolized medications. Brit. J. Clin. Pharmaco. 56, 588–599. https://doi.org/10.1046/j.1365-2125.2003.01892.x

Lide, D.R. (2001). CRC Handbook of Chemistry and Physics, 82nd Edition. Taylor & Francis. pp. 3–140.

Lieberherr, G., Auderset, K., Calpini, B., Clot, B., Crouzy, B., Gysel-Beer, M., Konzelmann, T., Manzano, J., Mihajlovic, A., Moallemi, A., O'Connor, D., Sikoparija, B., Sauvageat, E., Tummon, F., Vasilatou, K. (2021). Assessment of real-time bioaerosol particle counters using reference chamber experiments. Atmos. Meas. Tech. 14, 7693–7706. https://doi.org/10.5194/amt-14-7693-2021

Mahowald, N., Albani, S., Kok, J.F., Engelstaeder, S., Scanza, R., Ward, D.S., Flanner, M.G. (2014). The size distribution of desert dust aerosols and its impact on the Earth system. Aeolian Res. 15, 53–71. https://doi.org/10.1016/j.aeolia.2013.09.002

Maricq, M.M. (2008). Bipolar diffusion charging of soot aggregates. Aerosol Sci. Technol. 42, 247–254. https://doi.org/10.1080/02786820801958775

Martinsson, B.G., Karlsson, M.N., Frank, G. (2001). Methodology to estimate the transfer function of individual differential mobility analyzers. Aerosol Sci. Technol. https://doi.org/10.1080/027868201753227361

Naseri, A., Johnson, T.J., Smallwood, G., Olfert, J.S. (2023). Measurement of the centrifugal particle mass analyzer transfer function [Manuscript submitted for publication].

Payne, S.D., Symonds, J.P.R. (2022). Evaluation of various face covering filter materials using particles classified by aerodynamic diameter up to 5 micrometres. FILTECH 2022, Cologne, Germany. https://filtech.de/conference/conference-archive/

Sang-Nourpour, N., Olfert, J.S. (2019). Calibration of optical particle counters with an aerodynamic aerosol classifier. J. Aerosol Sci. 138, 105452. https://doi.org/10.1016/j.jaerosci.2019.105452

Tavakoli, F., Olfert, J.S. (2013). An instrument for the classification of aerosols by particle relaxation time: theoretical models of the aerodynamic aerosol classifier. Aerosol Sci. Technol. 47, 916–926. https://doi.org/10.1080/02786826.2013.802761

Tran, S., Iida, K., Yashiro, K., Yoshiko, M., Sakurai, H., Olfert, J.S. (2020). Determining the cutoff diameter and counting efficiency of optical particle counters with an aerodynamic aerosol classifier and an inkjet aerosol generator. Aerosol Sci. Technol. 54, 1335–1344. https://doi.org/10.1080/02786826.2020.1777252

Vasilatou, K., Wälchli, C., Koust, S., Horender, S., Iida, K., Sakurai, H., Schneider, F., Spielvogel, J., Wu, T.Y., Auderset, K. (2021). Calibration of optical particle size spectrometers against a primary standard: Counting efficiency profile of the TSI Model 3330 OPS and Grimm 11-D monitor in the particle size range from 300 nm to 10 μm. J. Aerosol Sci. 157, 105818. https://doi.org/10.1016/j.jaerosci.2021.105818

Xiao, K., Swanson, J.J., Pui, D.Y.H., Kittelson, D.B. (2012). Bipolar diffusion charging of aggregates. Aerosol Sci. Technol. 46, 794–803. https://doi.org/10.1080/02786826.2012.667585